DOE/MC/30086 -- 5397
Distribution Category UC-132

Naturally Fractured Tight Gas Reservoir Detection Optimization

Quarterly Report
July 1 - September 30, 1995

Work Performed Under Contract No.: DE-AC21-93MC30086

For
U.S. Department of Energy
Office of Fossil Energy
Morgantown Energy Technology Center
P.O. Box 880
Morgantown, West Virginia 26507-0880

By
Advanced Resources International, Inc.
1110 North Glebe Road
Suite 600
Arlington, Virginia 22201

Disclaimer

U. S. DEPARTMENT OF ENERGY
MORGANTOWN ENERGY TECHNOLOGY CENTER
QUARTERLY STATUS REPORT
FOR THE PERIOD
July 1, 1995 - September 30, 1995
DATE OF SUBMISSION: 10/20/95

CONTRACT NO:	CONTRACTOR:
DE-AC21-93MC30086	Advanced Resources International, Inc.
CONTRACT NAME:	**CONTRACT PERIOD:**
Naturally Fractured Tight Gas Gas Reservoir Detection Optimization	09/30/93 - 03/31/97

CONTRACT OBJECTIVE: No Change

TECHNICAL APPROACH CHANGES: No Change

1.0 HIGH-RESOLUTION AEROMAGNETIC SURVEY:

This study was commissioned by World Geoscience, Inc. (WGC) at the request of Advanced Resources International (ARI) as part of a project to interpret high-resolution aeromagnetic data in the southern Piceance Basin of western Colorado. This phase of the project includes the construction of a 1:250,000 scale depth-to-magnetic-basement contour map, as well as supporting documentation in the form of two-dimensional forward magnetic models of selected cross-sections of interest and a 1:100,000 scale interpretation of near-surface magnetic sources.

WGC flew a high-resolution aeromagnetic (HRAM) survey of the study area in late 1994. A qualitative magnetic interpretation was completed in early 1995. At ARI's request, WGC contracted Michal Ruder to perform a quantitative magnetic interpretation of the survey, with the goal of providing a magnetic basement depth contour map as the final deliverable product.

To complete the study, we have applied standard quantitative techniques to the HRAM data to derive the configuration of the basin's magnetic basement. Analysis of a representative set of profiles has been performed, using Peters and Demi-Pente depth estimation techniques. These results were tested by computing forward models along two key profiles. The final depth estimates have been contoured at a 0.5 km contour interval.

The magnetic basement depth map identifies regions of important basement relief as well as first-order regional fracture zones which may separate regions of different basement rock compositions. These regions of coherent basement 'fabric' represent basement blocks which can transmit stress in a 'uniform' fashion to the overlying sedimentary horizons. We would expect to see significant structural anomalies in the basin sediments near the proposed basement fracture or fault zones.

The deliverable products for this study include:

Magnetic basement depth contour map (1:250,000 scale)
Two-dimensional forward magnetic models of two profiles
Near-surface magnetic source interpretation map (1:100,000 - scale)

Zeev Berger of Berger Enterprises, Calgary, will work the next phase of the study with the ARI staff. This will include a synthesis of the magnetic basement depth map with the detailed examination of the short-wavelength, near-surface magnetic anomalies and their possible association with reservoir fractures and hydrocarbon migration.

1.1 Methodology

The study consists of three sections: interpretation of near-surface or supra-basement magnetic anomalies (1:100,000 scale), profile depth analysis of selected flight lines and tie lines, and two-dimensional forward modeling of selected profiles. Phase I, the interpretation of near-surface magnetic anomalies, is the only 'qualitative' part of the study. Phases II and III include computations which limit the range of depth and magnetic susceptibility for proposed magnetic sources in the study area.

Phase I included the study and comparison of the short-wavelength HRAM anomalies with mapped geologic structures of the Grand Junction and Leadville quadrangles, as well as a comparison of the magnetic data with published topographic maps. Positive and negative correlations were noted and mapped.

Phase II was the largest portion of the effort. It entailed the examination of every tie line and every tenth flight line for magnetic source depth estimation. The Peter's Half Slope and Demi-Pente techniques were used to compute magnetic depths. Generally, these procedures yield estimates which may be within 10% of the actual source depth. All depth estimates were posted on a 1:250,000 basemap, and an assumption of source geometry was imposed. Deep sources were usually interpreted as 'interface' solutions (i.e. contacts between two significant masses of different susceptibilities) and shallow, near-surface sources were interpreted as 'thin-sheet' solutions (i.e. dikes, sills, flows). These depth estimates were datumed to mean sea level and then contoured at a 0.5 km interval to produce to the depth to magnetic basement map.

Phase III provided verification of the depth to magnetic basement map in the form of 2 two-dimensional forward magnetic models across important structures in the basin. The

magnetic source depths from the basement map were used as input to the models and the resulting computed anomalies were compared with the observed magnetic anomalies along the profiles. This type of forward modeling was very effective for testing the depth estimation procedure.

Phase II: Magnetic Basement Depth Map

Figure 1 shows our interpretation of the relief which is present on the magnetic basement. This contour map is reflects the top of the iron-rich basement of the survey area; within this region there are several 'basement blocks' of varying magnetic susceptibility. The map shows important basement structural trends which have influenced the overlying basement rocks and exerted significant tectonic control on the structural development of the basin.

Several important basement blocks are readily identified on the magnetic basement contour map. These include the broad basement high in the south central portion of the study area and the NW-trending trough along the eastern portion of the basin. The southern high is part of an east-west trending regional structure which is well-known by workers in the Piceance. It is truncated on the east by the NW-trending trough, which is also the deepest part of the basin. The zone of truncation probably correlates with an ancient basement fracture zone. Note that the present day Grand Hogback runs parallel to this proposed fracture, suggesting that the eastern part of the basin is comprised of basement fabric which is dominated by NW-trending fractures and faults.

Perhaps one of most intriguing results of the depth to magnetic basement map is the trough or graben which is mapped on the north side of the south-central high. This part of the basin is appears to be a down-faulted structure and may present some interesting new hydrocarbon play concepts.

Magnetic depth estimation for the northwest portion of the survey has generated some high-confidence basement depth picks. However, the contouring of these depth estimates is problematic, as the shape of the survey coverage forces us to create a N-S contour bias. In reality, we believe that the basement structures in this area are more probably E-W.

1.2 Results

Phase I Interpretation of Supra Basement Magnetic Anomalies

The Piceance Basin HRAM data are characterized by two important types of features: 1) Strong amplitude, long-wavelength anomalies which reflect variations in basement iron composition and basement relief; and 2) Variable amplitude, extremely short-wave length anomalies which are sourced by iron-rich rocks which are very near the topographic surface. Earlier work in the area focused on the basement-related anomalies only. As part of this work, we wanted to map the short wavelength anomalies and compare them with mapped geology (as

presented on the Grand Junction and Leadville quadrangle geologic maps). Some of the ridge-forming horizons (Mesa Verde, particularly) have excellent correlation with magnetic anomalies. This indicates that there is significant iron present in portions of the Mesa Verde, and this may present an opportunity to use the HRAM data as a mapping tool for buried, faulted Mesa Verde structures. Conversely, other areas of dramatic topographic relief show no magnetic signature, indicating that these units (e.g. Book cliffs cliff-formers) are relatively non-magnetic. High-resolution aeromagnetic data will not provide insight into the location of buried non-magnetic units.

Not surprisingly, all of the mapped dikes correlate well with short-wavelength magnetic anomalies. The HRAM data suggest that there are additional unmapped (buried?) dikes in the region between Maam Peak and the Divide Creek Anticline. The area immediately north of the Divide Creek Anticline is partially covered by basalt-bearing alluvium. This zone appears as a region of chaotic or disrupted short-wavelength magnetic energy in the HRAM data. The depositional pattern of the alluvium may reflect underlying structures and should be studied and compared with seismic information.

Phase III: Two-Dimensional Forward Magnetic Modeling

The final part of the study included the testing and validation of the magnetic basement depth map. Two regional profiles were selected, to be used as calibration points for the depth estimation results. These profiles, cross significant magnetic anomalies in the basin. By limiting the depth of the basement, we can derive optimal magnetic susceptibilities for the individual basement blocks by using forward modeling techniques. This method highlights to the locations of basement fracture zones or zones of contact for basement blocks of different magnetic susceptibilities and rock compositions.

Profile 1, (figure 2) crosses NE through the dramatic NW-trending fracture zone discussed earlier. The model depicts a basement high in the SW which is characterized by intermediate to mafic composition (significant iron enrichment relative to felsic rocks). This is juxtaposed by a structural low in the NE, where basement rocks are highly felsic (and iron poor). The dramatic contrast in magnetic susceptibility between the two blocks generates the high-amplitude anomaly; the large amount of relief at this contact produces the change in anomaly wavelength at the contact.

Profile 2, (figure 3) trends West-East along the southeastern part of the study area. This region is less complex than Profile 1, but there is still significant variation in basement relief and magnetic susceptibility. Again, we can deduce basement rock composition from the modeled susceptibilities.

1.3 Recommendations for further study

In this study, we have applied standard interpretation and modeling techniques to gain a quantitative understanding of the magnetic basement in the southern Piceance Basin. The magnetic basement map has shown some surprising results, some of which may warrant further investigation with respect to their implications about hydrocarbon generation and migration.

Additional quantitative analysis will provide more definitive insights into basement relief, basement composition, and delineation of basement blocks. A feasible follow-on study for the 'graben' region could include two-dimensional forward modeling of 5 to 10 additional profiles. Modeled magnetic susceptibility variations in the basement can be mapped. This would a helpful tool for further delineation of regional structural blocks and tectonic elements.

The HRAM technology is very current, and it presents the opportunity for several important research development initiatives. A better understanding of the short-wavelength, near-surface component of the magnetic signal is critical, and this information may have direct bearing on hydrocarbon fracture plays. To pursue this avenue further, several projects should be undertaken: 1) There is virtually no information on magnetic susceptibilities for the sedimentary rocks in the Piceance Basin. In order to understand the short-wavelength anomalies, we must have concrete evidence for sedimentary magnetization. A field program should be developed to measure susceptibilities in situ and susceptibilities of available drill cores. This information- can be stored in an archival database which can be readily updated with new survey information; and 2) Many of the Piceance Basin survey's short-wavelength anomalies correlate strongly with variations in flight elevation. Currently, no aeromagnetic data acquisition contractor has a differential continuation operator in use to normalize aeromagnetic data acquired at varying elevations to a common (i.e. flat) datum. This mathematical operator is not a trivial development. Considerable time would be required to derive and test continuation algorithm, but it would be of great long-term financial benefit to both the acquisition companies as well as their exploration clients continuation.

2.0 FIELD PERFORMANCE SITE SELECTION

The site recommended for the seismic acquisition is the Rulison Field, over the MWX site, Piceance Basin. The reasons for this site to be preferred over all other possible sites include:

- The tremendous volume of information concerning the geologic setting, including fractures, stress, flow directions, stratigraphy, geologic history, and general nature of the rocks and stresses that they have been subjected to during geologic time. By adding our seismic data to what is already known, the amount of meaningful information that we can identify in our survey will be increased.

- The S-wave and P-wave VSPs that have already been acquired there during DOE - USGS - Sandia Lab research efforts. We plan to use this data to help us interpret our seismic data. The use of this pre-existing data saves us the expense of re-acquiring a 9C VSP in the area of our seismic acquisition.

- Barrett Resources has an active drilling and exploration program at Rulison Field. Their knowledge and expertise in re-completion and drilling will allow the seismic anomalies we identify to be evaluated by drilling, thus providing the final link in the standard chain of geologic study-geophysical evaluation-anomaly identification-production attempt.

We recommend that the seismic acquisition, detailed below, be accomplished at Rulison Field, to include the MWX site, in the Piceance Basin.

3.0 TECHNICAL WORK TO BE PERFORMED:

About 4 sq. miles of 3D seismic acquisition (Feb. 96), 9C vsp re-processing (spring 96), 2D 9C seismic line (fall 1996).

3.1 3D P-wave Reflection Seismic

1) Look for azimuthal variations in the seismic response that can be tied to well-control documentation of gas production from naturally fractured reservoirs, and

2) Find additional anomalies in well-bores that would reveal by-passed pay, and

3) Find undrilled anomalies.

P-wave sources (either vibrioses or dynamite) will be used, and vertical geophones (conventional geophones) for a conventionally acquired survey. What will be different is the processing: the data will be queried to determine the fast direction and the slow direction. These two directions will be tested against well control to see their relationship to the open natural fractures' direction. Theory predicts that the P-waves parallel the fractures sense the fast direction; while the P-waves perpendicular the fractures will sense the slow direction.

Conventional P-wave processing for 3D volumes will proceed: surface consistent amplitude adjustment, surface consistent deconvolution, statics estimation. The data will then be divided into two volumes: parallel and perpendicular the fractures (fast and slow directions). Velocity estimation will be azimuth-dependent. DMO will be run, followed by velocity estimation, stack, and post stack time migration. The AVO gradient for each volume for the events of interest will be calculated. The reflections of interest will be mapped, and their amplitudes, velocities, frequencies, and AVO signatures compared in map form.

Anomalies will be identified, and the well control tied to the seismic. In the fall of 1996, one 9C (3 sources, P, SH, SV, and 3 receivers, V, H1, H2) will record one 2D 3-mile line will be shot to document the relationship of the P-wave 3D anomalies to shear-wave reflection events, times, and polarizations. The quality of the P-S (mode-converted) reflections will also be studied to see if diagnostic information is retrievable from those reflections, when used in conjunction with the P-P reflection data. About half the profile will lie within the 3D volume, and the remainder will lie outside.

3.2 Vertical Seismic Profile

USGS and DOE publications on the VSPs acquired in previous investigations at the MWX site show the P-wave and S-wave time-depth arrivals, P-wave corridor stacks, and velocity data. If the tapes can be found, the data will be re-processed to determine the fast and slow shear wave directions, which will be compared to the fast and slow directions determined from the P-wave 3D seismic volume. The publications provide the bare minimum of required data for our project: the shear-wave and P-wave time-depth relationship for this area. With this information, we can identify the times of the important formation boundaries for S and P wave reflections. The re-processed volumes provide the preferred necessary data input for our project: the P and S wave time-depth-velocity-polarization information, and corridor stack data if possible.

3.3 2D 9C seismic line

In the Fall of 1996, after processing and interpretation of 3D seismic volume, a 9-component (P, crossline shear wave, and inline shear wave sources; each recorded by 3-component geophones) 2 mile line will be recorded, in order to show the relationship between shear wave anistoropy, related to fracture density and fracture orientation, and well control, and P-wave seismic response. The location of the seismic line will be determined by the geologic control, and the nature and location of P-wave seismic anomalies.

4.0 SEISMIC ACQUISITION PROCESSING AND ASSOCIATED COSTS

As described above we propose to acquire and process (or reprocess) three data volumes during the performance of this Test Plan: the conventional 3D survey of approximately four square miles will be acquired in the second quarter of FY96. The cost for this survey, based on preliminary contractor bids is on the order of $230,000. This figure includes permits and processing. The VSP tapes from the MWX site have been located and pending administrative coordination, reprocessing can begin upon test plan approval. Cost of the reprocessing of this data is approximately $40,000. Lastly we propose to acquire a two mile shear wave line as indicated on Figure 1, during the fourth quarter of FY96. Current estimate of acquisition and processing costs are approximately $190,000. This bid includes permits and processing, and

incorporates standard shear wave vibrators. Should depth penetration of the IVI minivibs be adequately demonstrated prior to this line being acquired the utilization of these minivibs would reduce the 2D line cost by approximately $100,000 to only $90,000 allowing us to double the line length to 4 miles or acquire two lines of 2 Miles each. Total cost for the three data volumes is currently estimated at $460.000.

4.1 Conventional 3D Survey

Approximately four square miles of conventional 3D P-wave seismic data, as described below and as indicated on Figure , would be acquired in the second quarter of FY96. This data would be acquired with sufficient fold to ensure adequate offset range and variable azimuths to insure suitability for azimuthally dependent AVO applications. Recording parameters follow below:

Source:	Dynamite, 25# @ 60', one hole, double capped
Source Spacing:	220 Feet
Source Line Spacing:	1320 Feet
Source Line Orientation:	N70W
Total Number of Sources:	559
Receiver Station Interval:	220 Feet
Receiver Line Spacing:	1100 Feet
Receiver Array:	Circular, 20 to 30 Foot diameter centered on flag
Total Number of Receivers:	695
Receiver Line Orientation:	N-20-E
Average Fold:	54
Average Fold Split Azimuth:	28

Acquisition timing requires that NEPA preparation begin in November, 1995 and permitting and shot hole drilling begin in December of 1995. This would allow recording to begin in February of 1996. Acquisition should be completed during February. Processing is expected to be completed by May of 1996 with concurrent interpretation which will be completed in July of 1996.

4.2 VSP Reprocessing

We plan to reprocess a multicomponent VSP acquired at the MWX site. Although evaluated by the USGS, this data has not received benefit of modern shear wave and P-wave VSP processing algorithms. Reprocessing is expected to begin after test plan approval and upon receipt of the raw data. Completion of processing is expected approximately two months after receipt of the data, again with concurrent interpretation which will be completed two months after completion of processing.

4.3 2D Shear Wave Line

We propose to acquire the 2D shear wave data line in September of 1996. Acquisition should be completed in September. Processing is expected to be completed in November of 1996. Interpretation will occur concurrently and be completed and integrated into the overall seismic interpretation by December, 1996. Recording Parameters follow below:

Source:	3M Shear Minivibs T15,000 or Buggy or IVI minivib
Source Spacing:	220 Feet
Line Length:	10,560 Feet
Line Orientation:	TBD
Total Number of Sources:	96
Receiver Station Interval:	220 Feet
Receiver Array:	Podded or Circular, 20 to 30 Foot diameter centered on flag with all phones buried.
Total Number of Receivers:	96

5.0 THEORETICAL BACKGROUND CONCERNING P-WAVE MULTI-AZIMUTH 3D SEISMIC

5.1 Normal Moveout Velocity

Crampin (1985, 1991) published predicted velocity variations as a function of azimuth to the crack for P-waves (and S-waves).

Figure 1A (from Crampin, 1991) shows A) P wave velocity variation for layer anistoropy: no variation in azimuth. Z is vertical propagation, N is North and E is East. A 7% layer anistoropy for the shear-wave velocities was specified by Crampin as present, but using the numbers off the plot, a 10% S wave velocity is observed, using the equation ((max VS - min VS) / max VS),

The VP layer anistoropy observed on the plot is 8%, in that the vertical velocity is less than the horizontal velocity.

Figure 1B shows the variation in velocity for P and S waves, for only vertical cracks in a medium, no layer anistoropy effect, and the cracks are striking E/W. The cracks are water-filled. Perpendicular to the cracks (to the North) the P-wave velocity reaches a minimum at ~45 degrees. Parallel the cracks (to the East) the P-waves travel more quickly and show no variation with angle of incidence. While perpendicular to the cracks at the farther offsets encountered in reflection data, that is, angles of incidence between 15-30 degrees, the P-waves travel more slowly.

Figure 1C (from Crampin, 1991) shows the effect of layer anistoropy plus crack anistoropy. There, the variation of VP with azimuth is not very marked, due to the interaction of the effects of the layers and the cracks. If one were to change the relative percent of layer anistoropy and crack anistoropy, and/or the contents of the cracks, then the relative appearance of the curves would change.

Figure 1D is my calculated output from ANISEIS, a seismic modelling code that allows the calculation of seismic wave velocities in anisotropic media. It shows the effect of 10 degree layer dip in the X direction with (subsequent) vertical gas-filled cracks introduced, striking perpendicular to the X direction. The layer anistoropy for VP is $\sim 5\%$. The crack density is 7%, which is a moderate crack density. Because the cracks are parallel to the Y axis, the Z-Y plane does not see the effect of the cracks. The X-Z plane sees the effect of the cracks at the far offsets, and the velocity is decreased.

Figure 2 (from Crampin, 1985) plots VP and VS as a function of the angle of incidence, for one azimuth of propagation: perpendicular to the cracks. It compares the effect of gas in the cracks (a), to liquid in the cracks (b). Vertical propagation is indicated by the "90". Gas in the cracks magnifies the effect of the slow down in the velocity (perpendicular to the cracks).

Other workers have predicted attenuation anomalies (Gelinsky and Shapiro, 1995) by azimuth for P-waves, in the presence of vertical oriented fractures.

Gibson and Toksoz (1990) predicted the permeability variation with direction in fractured rocks from seismic velocity anistoropy.

Mavko et al. (1995) present a method to predict stress-induced seismic velocity anistoropy in rocks. When discussing P-wave velocity anistoropy, arguments about stress-induced or crack-induced velocity aniostropy may arise. When unequal horizontal stresses are present, the cracks approximately normal to the maximum horizontal stress are more closed, compared to the cracks approximately parallel to the maximum horizontal stress. Thus, one direction looks "stiff" to propagating P-waves (the direction of maximum horizontal stress); while the orthogonal direction looks "compliant" (minimum horizontal stress direction). Mavko et al.'s method is stated to be "relatively independent of any assumed crack geometry and is not limited to small crack densities." Our approach to the field data will be to start at the wells with the production history, the pressure data, the cumulative production records (first 6 months, first 12 months, total cum.), tie the production data to the seismic data, and evaluate the relationships observed. A large first 12 month cumulative production, in tight matrix rocks, implies a substantial fracture assist. Therefore, the relative crack density is assumed to be proportional to the quantity of production (normalized by time under production). We also will evaluate number of years (or months) that each well has been under production, prior to the data acquisition, in order to see if a drop in pore pressure, due to production, has allowed the cracks to close somewhat, thus decreasing the "seismic anomaly". The seismic anomalies to be evaluated are listed in this paper.

5.2 AVO dependent upon azimuth

Since the P-wave amplitude variation with offset (AVO) is governed by the contrast in P and S velocity, at the appropriate angle of incidence of the P-wave, as the P and S velocity varies with angle of incidence and with azimuth, so will the AVO response.

The layer anistoropy is present to increase (usually) the P and S velocity with increasing angle of incidence. This increase in VP and VS is the same for all azimuths, though (azimuth-independent) in flat-lying rocks.

The crack anistoropy is "invisible" parallel to the cracks, because the P-wave velocities are not affected by the cracks, and the SV (the in-line S-polarization) is S1, the fast shear wave, which is insensitive to the crack density. Perpendicular to the cracks, however, the P wave velocity is reduced on the farther offsets, and the SV is the S2 or slow shear wave, which is the sensitive shear wave to the cracks.

Mallick and Frazer (1991) used model data to show that the P-wave AVO depends on the azimuth of the shot line with respect to the vertical fractures' strike. They present a way to calculate the reflection and transmission coefficients for azimuthally anisotropic media, and use this code to calculate the synthetic seismograms from which they plotted the reflection coefficients as a function of offset, for different shot line directions relative to the fracture strike.

5.3 Amplitude dependent upon azimuth

Stacked data may exhibit different amplitudes with azimuth due to a different AVO with azimuth.

Dong and McMechan (1993) discussed a 3-D prestack migration algorithm suitable for anisotropic media. They presented model data in which "zones of anomalous directionally dependent reflectivity associated with anisotropic fractures zones are detectable in both the 3D common-source data and the corresponding migrated images." They point out that reflectivity has a directional dependence in anisotropic media. If partial azimuth images are stacked, the stacking obscures most of the directional reflectivity information in the images. "Detection and interpretation of such anistoropy-related effects require analysis of individual images from common-source gathers that illuminate the target in independent directions". We agree with Dong and McMechan that analysis of individual (independent) narrow-azimuth images provide the ability to detect and characterize the directionally dependent reflectivity. However, the more practical way to accomplish this is to separate a 3D volume into two azimuths, parallel and perpendicular to the dominant open fracture azimuth, correctly process both volumes through stack and migration, and then compare the amplitudes, velocities, frequencies, and AVO signatures present in the two volumes.

5.4 Frequency - Attenuation dependent upon azimuth

Akbar et al. (1993) published that the attenuation anistoropy rather than velocity anistoropy is strongly correlated with permeability. They stated that "in the case when a plane P-wave propagates perpendicular to the pore orientation, the attenuation, (Q^{-1}_{90}), is always higher than when a wave propagates parallel to this orientation, (Q^{-1}_{0}). The ratio of these two attenuation values (Q^{-1}_{90})/(Q^{-1}_{0}) increases with an increasing pore radius and decreasing frequency and saturation."

Gelinsky and Shapiro (1995) also showed in model data a significant azimuth-dependent attenuation effect (frequency-dependent attenuation) in P-wave seismic when vertical aligned fractures are present.

5.5 Travel time

If, after stack, different traveltimes with different azimuths are observed for P-wave data, then the effect of dipping sedimentary layers, and/or dipping cracks, may be investigated.

Normal moveout followed by stack is the P-wave processing step that corrects the offset data to the zero offset travel time, so that upon stack (vertical summation across the offsets), the signal is enhanced (stacked in phase), while noise is reduced (noise amplitudes are out of phase).

If after stack, different travel times are observed, then that indicates that the "zero offset time" is different for the different azimuths. See discussion below about phase.

5.6 Phase

Phase is a rather difficult quantity to deal with in real field data, while it is easy to deal with in model data of low complexity.

If there is a single reflection coefficient (one boundary), then a wavelet convolved with that reflection coefficient can be easily inspected for zero phase, 90 phase, 180 degree phase, etc. If there are a series of widely spaced reflection coefficients, such that their spacing is greater than the wavelet length (usually about 100 msec), then each reflection has only one wavelet present. Therefore, the phase of each reflection can still be reasonably discussed, and so can any "phase changes" observed throughout the section.

However, real field data have many reflection coefficients within 100 msec such that the reflections recorded are composite reflections containing interference phenomena. Therefore it is difficult to untangle geologic (stratigraphic) variation in the layer thicknesses and velocities from phase changes due to anisotropic attenuation.

It is possible that after stack, if differences in travel times are observed, the question could be posed, "Would phase shifting one section achieve a better "match" to the other azimuth?" Tests could be performed to investigate this concept.

6.0 FIELD DATA EXAMPLES OF P-WAVE MULTI-AZIMUTH DATA

6.1 Strike vs. dip

From O'Connell et al., 1993:

"In the spring of 1988, Shell acquired two orthogonal 3D surveys at Prospect Bullwinkle, located in the Green Canyon area of the Gulf of Mexico, to aid the development program which began later that year. Two surveys were acquired because of the complexity of the salt structure in the vicinity of the prospect. The independent acquisition and processing of two surveys shot perpendicular to each other provided a unique dataset for checking the quality and accuracy of standard 3D techniques. The high development cost of this deep water (410 m) turbidite field supported the acquisition of 2 3-D datasets to provide a valuable redundancy for stratigraphic interpretation.

This large scale 3D experiment has been analyzed in terms of interpretive impact. Detailed comparisons of the seismic images away from the salt complex show good agreement between the two surveys and verify the relative accuracy and repeatability of the acquisition, processing, and interpretation techniques. Structural comparisons between the survey s show that acquisition oriented in a strike direction to the primary salt face yields a superior sediment image, particularly near overhung salt. An examination of the effects of shooting direction on small scale stratigraphic resolution illustrates the importance of fine sampling in the dip direction to the features of interest. Amplitude maps extracted for the main bright spot level show differences in areal continuity that are large enough to affect the geologic model of the prospect."

"The main conclusion drawn from the comparisons of the two 3D surveys at Bullwinkle is that the interpretation of an prospect can be influenced by shooting direction. Hence it is very important to match the shooting direction to the geology. the lessons we learned from the analysis of the 3D experiment are:

1. The comparison of the two surveys demonstrates the repeatability and basic accuracy of the acquisition and processing techniques employed at Bullwinkle. Shallow fault terminations and the oil water contact at the main pay accumulation occur at the same trace location [to within 100 ft] on both surveys, thereby supporting the estimated navigation accuracy.

2. Significantly improved imaging is obtained with data shot strike to the overhung salt face on the western side of the accumulation. This is interpreted to be due to differences in the degree of raypath distortions caused by salt, and by both vertical and lateral velocity gradients for the two orthogonal acquisition directions.

3. Differences in the resolution of the individual J sand lobes, and the imaging of the unconformities and sediment/salt onlap are also found to be influenced by shooting direction. In these cases it is believed that the coarse crossline sampling is the predominant cause of the observed effects. The resolution, as determined from well ties, comparison to VSPs, and a general interpretability, is superior in the inline direction, which has a 50 ft trace spacing vs. a 150 ft crossline sampling.

"Perhaps the most significant benefit of having two surveys is the redundancy they provide for high-cost deep-water development projects such as Bullwinkle."

Jim O'Connell, Shell, New Orleans, spoke at the GSH Jan. 11, 1995; see Appendix A for notes from that session.

What is different about Bullwinkle is that in the marine setting, the acquisition was actually accomplished in two separate passes, so that navigation and positioning of the survey needed absolute accuracy in order to tie the two surveys. Our survey will use the same phones and same sources: only in the processing center will the two volumes be separated for processing and analysis. This will remove two possible sources of error or variation: location (of sources and receivers) and coupling of sources and receivers to the earth. The coupling will be identical.

6.2 Azimuthal anistoropy

6.2.1 NMO- velocity: CGG - 1990 SEG - Silo Field, CO

CGG in the SEG 1990 Convention presented that they were able to determine fracture azimuth from their P wave reflection dataset. (See Garotta et al., SEG Expanded Abstracts, 1990, p. 1086 ff.) The particular P wave dataset was the 3-D three-component seismic reflection data gathered over the flat-lying sedimentary rocks of Silo Field, western United States. (See Martin and Davis, cited above, 1987.) The P wave reflection travel times were increased, due to a velocity decrease, on the far-offsets perpendicular to the vertical aligned fractures at Silo Field. The mid- to far-offsets on the P wave lines parallel to the cracks had minimum traveltimes, due to sensing a faster velocity field, compared to the mid- to far-offsets on the P wave lines perpendicular to the cracks. CGG's findings are consistent with theory which predicts a velocity decrease on the mid to far offsets normal to the cracks (perpendicular to the cracks) (see Crampin, 1985). The P wave vertical travel paths on any surface seismic line are not affected by vertical aligned cracks. (They are affected by dipping cracks, said ARCO's Jim

Gaiser in the 1987 SEG convention workshop, but the dipping cracks set up a symmetry in the rocks that is very difficult to unravel at this time.)

The P-wave lines perpendicular to the cracks are the ones to examine for effects due to high fracture density. The P-wave lines parallel to the cracks are diagnostic to look at the structure, or lithology: that is, to "ignore" the cracks and see only the "rocks". For interpretation, it is necessary to see both the uncracked rock response, and the cracked rock response, in order to compare the difference. In one direction, the bulk of the response is caused by the rock plus the cracks; in the other direction, the bulk of the response is caused by only the rock.

6.2.2 AVO - Bluebell Altamont (P-wave by azimuth)

Many basins in the Rocky Mountain basins, as well as other places, contain naturally fractured gas reservoirs. Production from these reservoirs is controlled primarily by the shape, orientation and concentration of these fractures. The detection of gas filled fractures prior to drilling can therefore greatly benefit the field development of the reservoirs. The objective of this project was to test and verify specific seismic methods to detect and characterize fractures in a naturally fractured reservoir. The Upper Green River tight gas reservoir in the Uinta Basin, Northeast Utah was chosen for the project as a suitable reservoir to test the seismic technologies.

Knowledge of the structural and stratigraphic geologic setting, and estimates of the in-situ stress field, were used to guide the acquisition and processing of approximately ten miles of 9-component seismic reflection data and a 9-component VSP. Three sources (P-wave, in-line S-wave, and cross-line S-wave) were each recorded by 3-component (3C) geophones, to yield a 9-component dataset. Evidence of fractures from cores, borehole image logs, outcrop studies, and production data, were integrated with the geophysical data to develop an understanding of how the seismic data relate to the fracture network, individual well production, and ultimately the preferred flow direction in the reservoir. The multidisciplinary approach employed in this project is viewed as essential to the overall reservoir characterization, due to the interdependency of the above factors.

Seismic anistoropy was observed in both the VSP and the reflection seismic data sets, and this anistoropy is considered to be a characteristic feature of the fractured reservoir under study. A clear relation was observed between fracture density, dominant fracture azimuth, and compressional (P) wave and shear (S) wave seismic properties, in the fractured Upper Green River gas reservoirs.

From the S-wave seismic, the fracture azimuth was inferred from the fast shear wave (S1 after rotation) direction, N40W, which indicates the stiff direction within a rock. The nature of the S-wave anistoropy with depth from the 9-C VSP revealed that no change in the orientation of the principal axes of the anistoropy was detected from 2800-8650 ft. (through the target reservoir zone at 6500-8650 ft): the dominant fast direction is N40W and the slow direction is

N50E. The S1 direction, calculated independently for the VSP and the surface S-wave data, gave similar results to within 15 degrees. The average S1 direction was consistent with geologic evidence of the dominant open fracture strike and the maximum horizontal compressive stress direction for this reservoir. Relative fracture density was estimated from the travel time anistoropy in the split shear wave data. Also, amplitude variations in the S2 shear wave component correlated with known fractured gas production.

Differences in the P-wave amplitude variation with offset and azimuth (AVOA) for gas-producing intervals known from wells were observed for the two seismic lines. Where the P-wave line direction was perpendicular to the fracture strike, AVO sensed the gas-filled fractures, whereas on the P-wave line whose direction was parallel to the fracture strike, the AVO was insensitive to the gas-filled fractures. The P-wave observations of low Poisson ratio intervals, that is, intervals that indicate a presence of gas in the rock, correlate with the S-wave indications of high fracture density.

The good correlation between the P-wave and S-wave results documents that P-wave AVO data can be used to evaluate the potential for gas in naturally fractured reservoirs, when the line is perpendicular to the fracture strike. However, the combination of P-wave and S-wave data adds a degree of certainty to the extraction of fracture characteristics from the seismic data. This work is being extended to 3-D P-wave surveys, such that a 3-D P-wave grid acquired along the principal azimuths (i.e., parallel and perpendicular to the gas-filled fracture strike), may be used to map high-fracture intensity zones within the 3-D survey area, using P-wave AVOA (amplitude variation with offset and azimuth). The calibration of the principal azimuths in depth with an S-wave VSP is strongly recommended.

7.0 3 D Basin Modeling

7.1 Two-dimensional basin simulator: Improvements continue to be made on the CIRFU and DataU modules used to input new information into the chemical kinetics and thermodynamics data banks. The code was tested in collaboration with Phillips Petroleum to determine its performance in problems involving precipitated (diagenetic) seals, so as to verify the robustness and correctness of the mass transport features.

7.2 Three-dimensional basin simulator: Work is completed on optimizing the visco-plastic solver and integrating it with the three-dimensional simulator. Preliminary testing of the integrated code has also been completed.

Much of the work is completed on improving our AVS visualization modules that allow us to view two-dimensional vertical and horizontal slices through the basin at a given time, as well as three-dimensional images of sedimentary units at a given time, as well as three-dimensional images of sedimentary units at a given time in the basin history. Improvements made include a flexibility to choose from a variety of variables to display. A superimposition of well locations, is now also included to allow for more precise checking of the input

stratigraphy with well data. Futhermore, we have developed a module for illustrating isosurfaces for arbitrary user-defined CIRFB variables (for example, porosity or grain size values).

The pressure and temperature modules have been made significantly more stable and efficient by using fifth order time discretization and projection techniques. Preliminary results to test these features and their integration into CIRFB have been obtained.

7.3 Data analysis and data base: Work continues on preparing more well data for input files, in order to achieve better well control in the southern part of the basin. Well files have been updated to include lithologic identity, as well as a unit number, which allows better correlation of stratigraphic units across the basin.

A six-part lithologic code was developed to add genetic information to the stratigraphic data for the Piceance Basin. This code distinguishes marine versus nonmarine units and comprises the following: hiatus; nonmarine sandstone; nonmarine shale; coal; marine sandstone; and marine shale. This coding should also expedite the data checking and quality control effort by allowing easy inspection for the three-dimensional stratigraphic module for the appropriate distribution of marine and nonmarine units throughout the basin.

Sequence stratigraphy data contributed by Roger Tyler and Ron McMurry (personal communication) from the Texas Bureau of Economic Geology was entered into electronic files. These data consisted of the depths in 33 wells of three mappable sequence boundaries, the maximum flooding surface and the flooding surfaces at the top of Unit 1 and Unit 2 (Tyler and McMurry, 1995). These data are being used for correlating genetic an litholgic units across the basin and for increasing the density of well control.

Data has been collected on textural variables for sandstone and shale, such as porosity, grain size and composition, and is being collected for carbonate rocks to be used to fit curves for rock failure parameters.

7.4 Organic reactions and multi-phase flow: Work continues on testing of the multi-phase reaction transport module for two-phase, two-component flow. The three dimensional curvilinear coordinate descriptizaiton numerical simulator has passed preliminary tests that illustrate its ability to preduce methane from source rock, generate a gas phase, and have this phase be expelled through overpressuring and finally to migrate via buoyancy.

A simple algorithm to account for generation of methane from maturation of organic matter has been developed and is being tested. It is being added to the multi-phase reaction-transport module.

8.0 Technology Transfer:

Project objectives and results to date were presented to the Colorado Oil and Gas Association on August 9, in Denver, Colorado. A review of project deliverable were made to DOE officials and their contractors in charge of operating the Naval Oil Shale Reserves (NOSR) at Casper, Wyoming office and DOE headquarters in Washington, D.C. The meetings were requested by DOE to determine project data and interpretations value regarding sale of NOSR properties in the Piceance Basin.

OPEN ITEMS: None

A. David Decker, Vice President

Figure 1

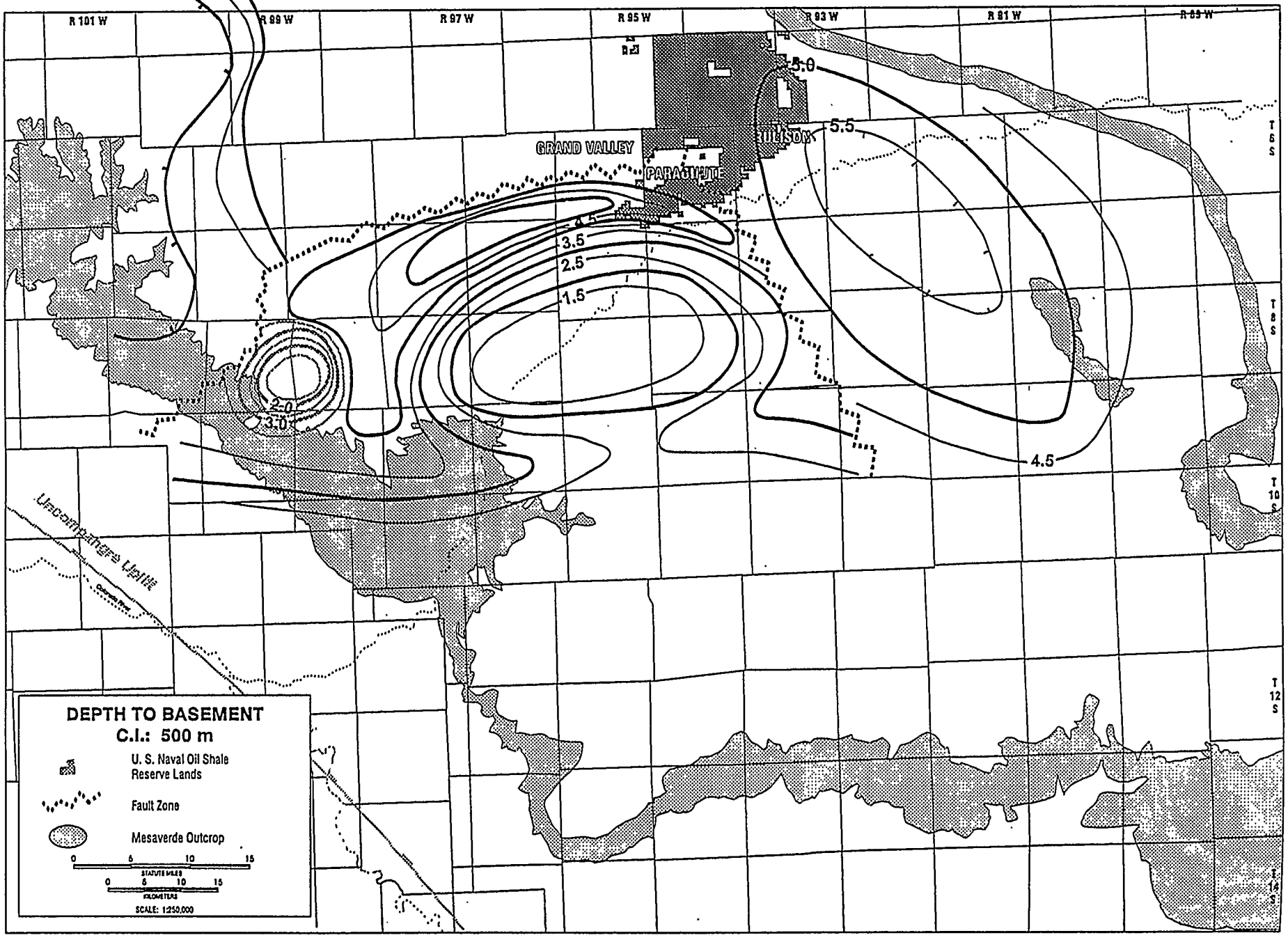
R 101 W
R 99 W
R 97 W
R 95 W
R 93 W
R 91 W
R 89 W
1.0
2.0
5.0
5.5
GRAND VALLEY
PARACHUTE
BULLSON
4.5
3.5
2.5
1.5
2.0
3.0
4.5
T 6 S
T 8 S
T 10 S
T 12 S
T 14 S
Uncompahgre Uplift
DEPTH TO BASEMENT
C.I.: 500 m
U. S. Naval Oil Shale Reserve Lands
Fault Zone
Mesaverde Outcrop
0 5 10 15
STATUTE MILES
0 5 10 15
KILOMETERS
SCALE: 1:250,000

Figure 2 : Two-Dimensional Forward Magnetic Model of Profile 1 (see Depth to Magnetic Basement Map for profile location of this SW to NE profile): The computed curve matches the observed total intensity magnetic anomaly curve quite well. The model shows shallow basement on the SW and deep basement on the NE; additionally, the shallow SW region is more intermediate to mafic in composition and the deep NE basement is more felsic and iron poor. The proposed graben discussed in the text is shown just to the west of the first-order fracture zone; it is highly mafic.

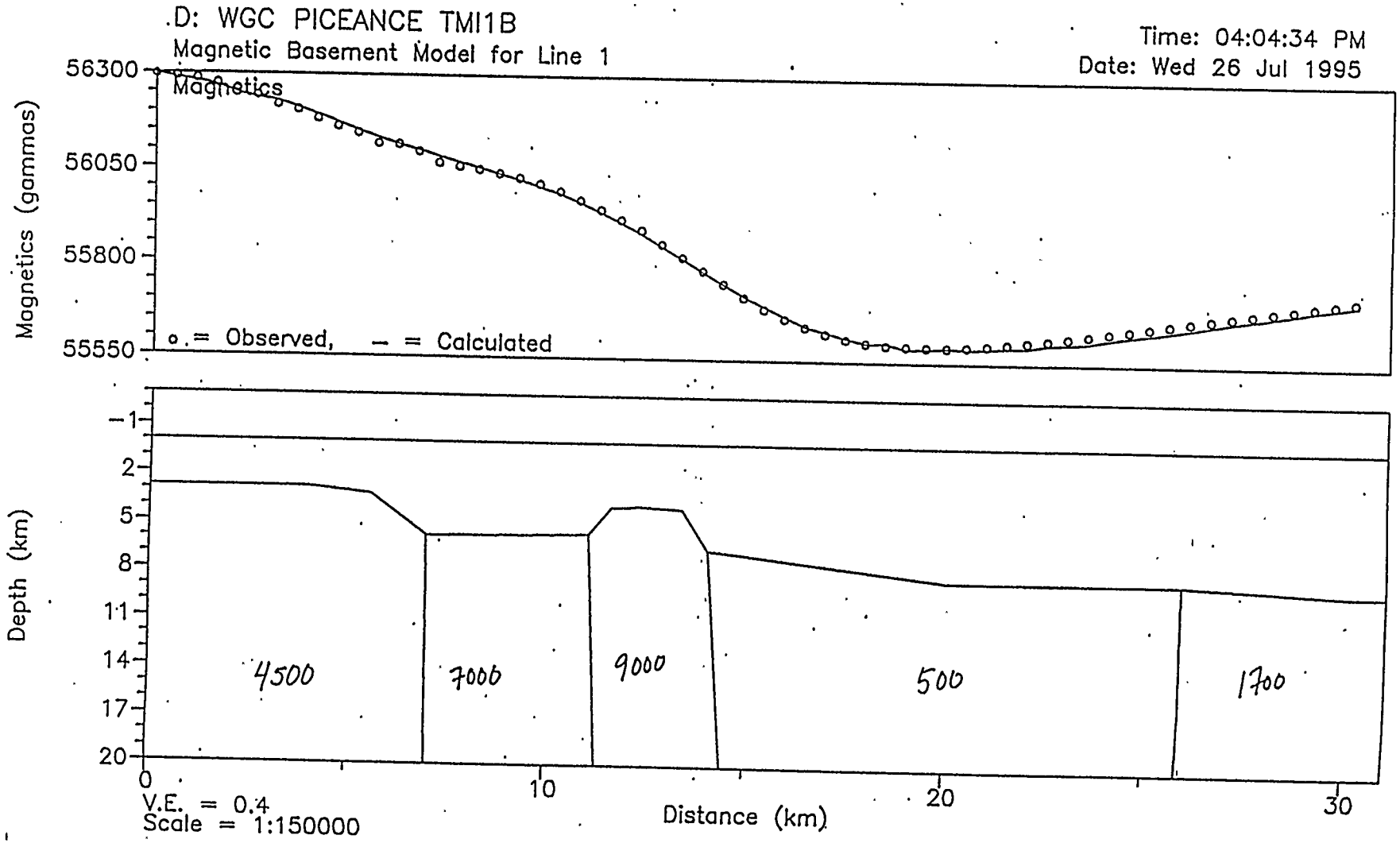

Figure 3 : Two-Dimensional Forward Magnetic Model for Profile 2: This west-to-east profile does not have so much basement relief as Profile 1. The western block, part of the south-central basement high, appears to be of intermediate composition. The eastern blocks, which are progressively deeper, have more felsic susceptibilities. They do not appear to be associated with the highly mafic material which underlies the thickest part of the basin (directly north of this profile).

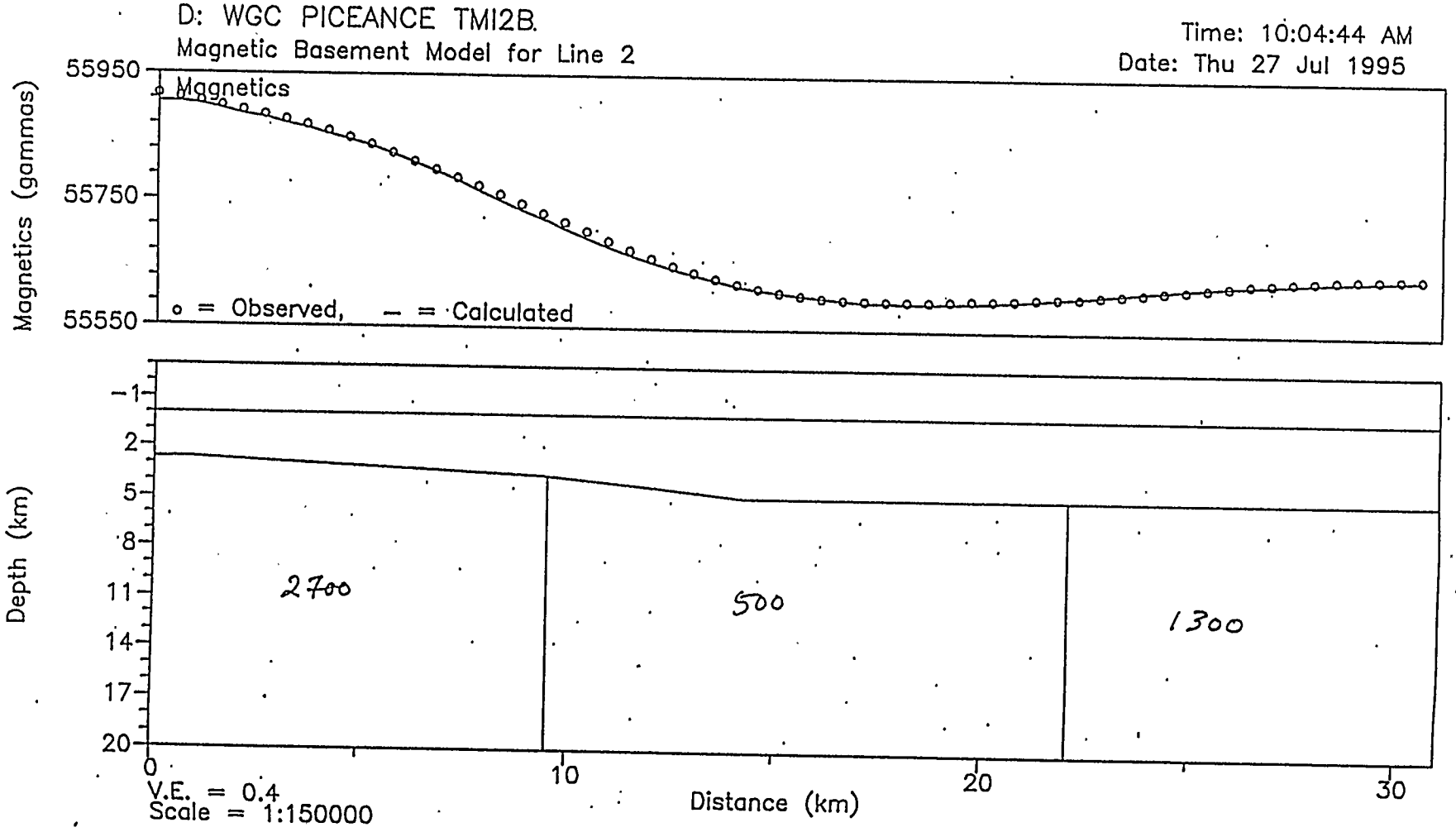

Figure 4

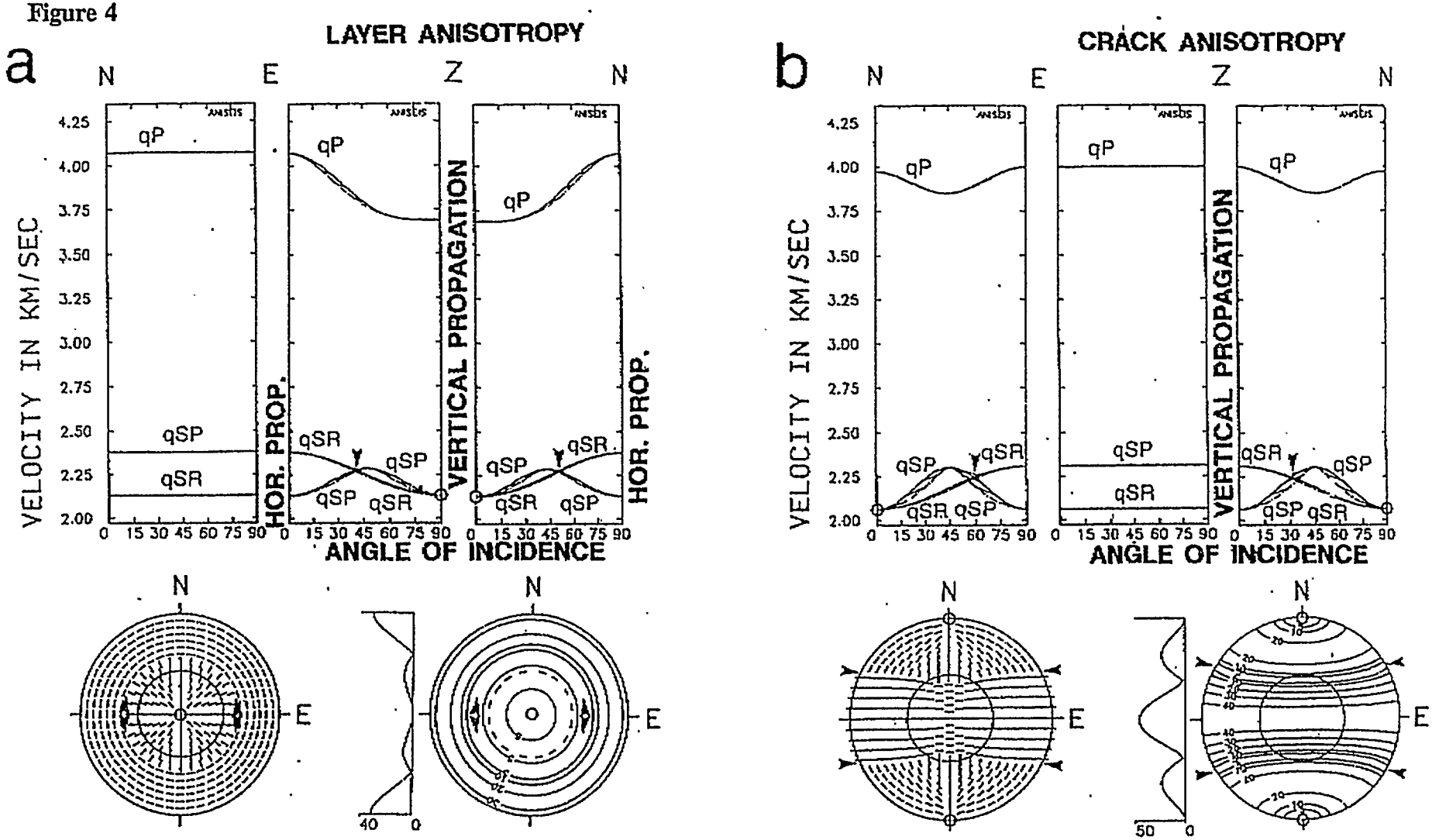

. Properties of (a) P07, with PTL anisotropy, and (b) C10, with EDA anisotropy where the vertical cracks strike east–west. Upper diagrams are velocity variations in the three mutually orthogonal symmetry planes: (N)orth–(E)ast; (E)ast–(Z)Vertical; and (Z)Vertical–(N)orth; where the upper solid lines are phase velocity, and the lower dot–dash lines are group velocity joined to the appropriate phase velocity every 10°. The three body waves are a quasi-*P*-wave, *qP*, and two quasi-shear waves, *qSP*, polarized (p)arallel, and *qSR*, polarized at (r)ight angles, to the symmetry plane through the symmetry axis (direction 0°). Lower diagrams are, to the left, equal-area projections (polar maps) of a hemisphere of directions of the phase-velocity polarizations of the faster split shear wave, *qS1*, and to the right, the delays between the split shear waves contoured in ms km^{-1}. (Note that in symmetry planes, as in the velocity variations the polarizations of *qS1* are sometimes *qSP* and sometimes *qSR*.) The inner circle (dashed in the contour diagrams) is the theoretical shear-wave window for the free surface at an angle of incidence 35.3°, and is inserted to give some internal scale. There is a north–south section of the delays to the left of the contoured projections. Kiss singularities are marked by open circles, and the directions of line singularities are indicated by arrowheads.

from Crampin, 1991

Figure 4C

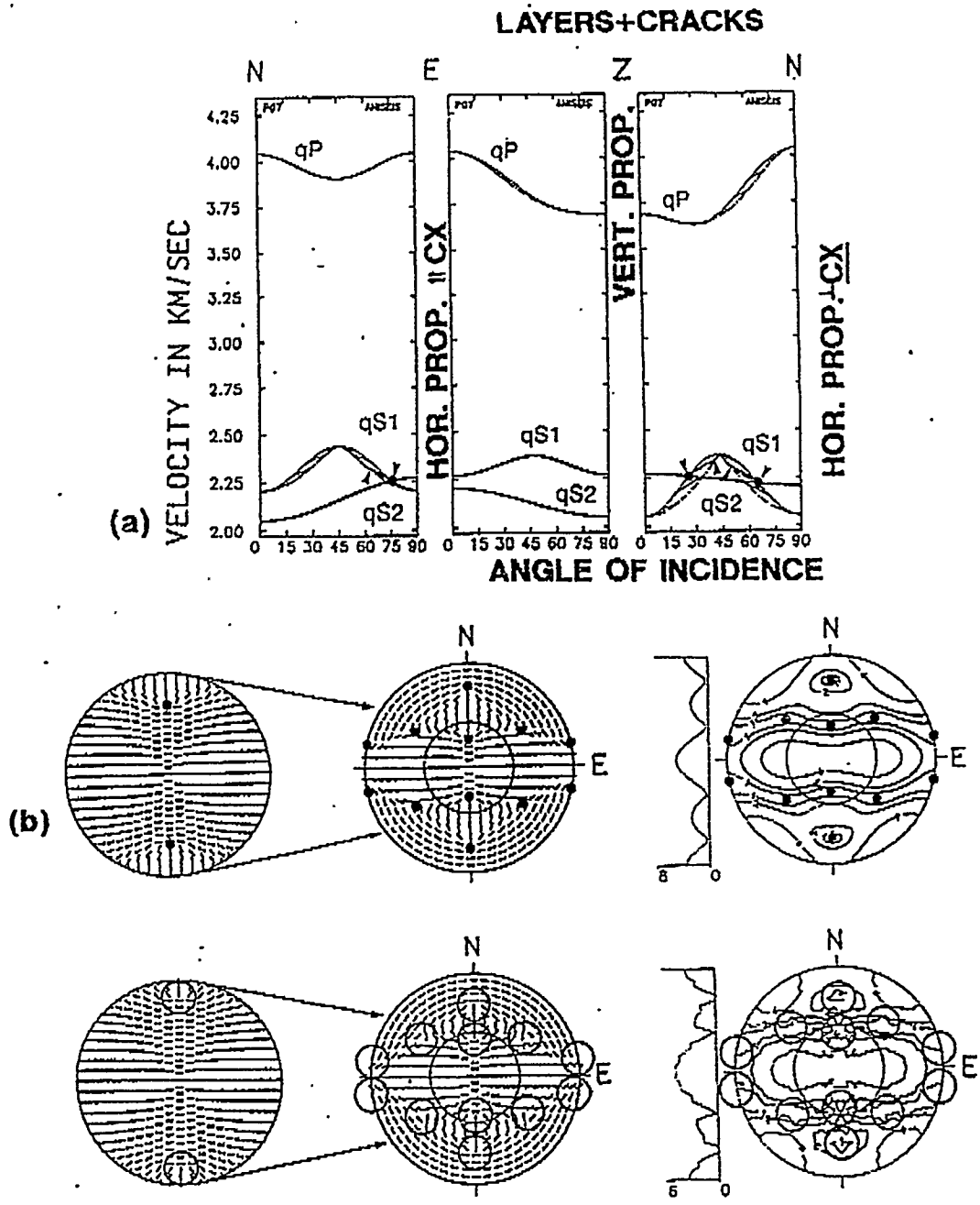

Properties of P07C10 with orthorhombic symmetry: (a) velocity variations in three mutually orthogonal symmetry planes, and equal-area projections of (b) phase-velocity, and (c) group-velocity variations. The irregular contours in (c) are discussed in the text. Notation as in Fig. 3. Solid circles mark the positions of point singularities on the phase-velocity variations in (a) and (b). Open circles mark schematically the centres of the anomalies on the group-velocity variations in (c). There are insets of the shear-wave window to the left of the equal-area projections of the polarizations.

from Crampin, 1991

Figure 4D

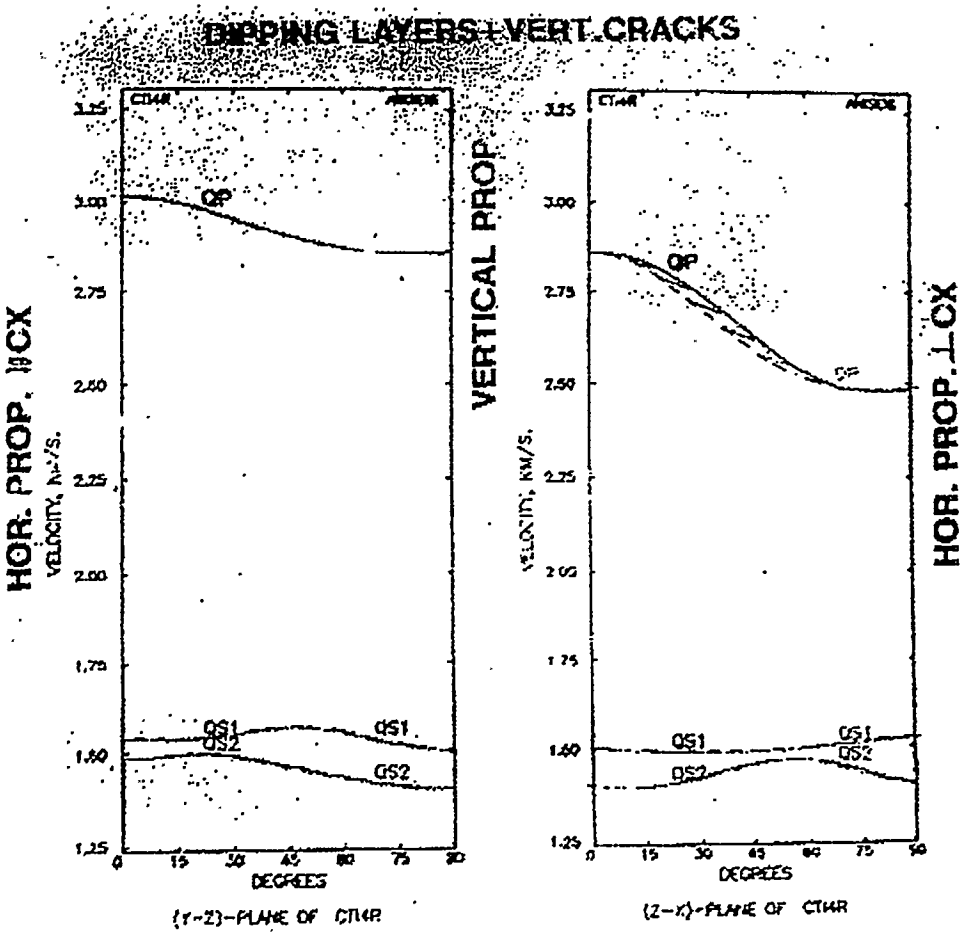
DIPPING LAYERS+VERT.CRACKS
HOR. PROP. ∥CX
VELOCITY, KM/S.
VERTICAL PROP.
HOR. PROP.⊥CX
QP
QS1
QS2
DEGREES
(Y-Z)-PLANE OF CTHR
(Z-X)-PLANE OF CTHR

FOR VERTICAL CRACKS

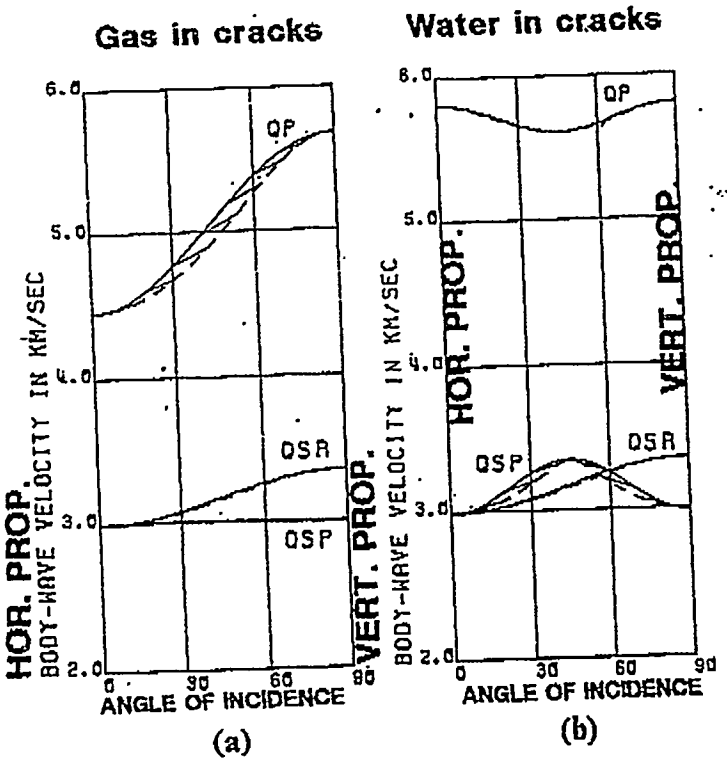

FIG. 2. Variation of seismic velocities through parallel cracks. Phase velocities (solid lines) and group velocities (dashed lines) for plane waves with angles of incidence between normal (0 degrees) and tangential (90 degrees) to distributions of parallel cracks with crack density 0.1 (other parameters in Table 2). The phase and group velocities are joined at every 10 degrees of phase velocity direction. The *qP*- and *qSP*-waves are polarized parallel, and the *qSR*-waves polarized at right angles to the incident plane through the axis of symmetry normal to the cracks. (a) dry cracks—HCD1; (b) cracks saturated with liquid—HCS1.

from Crampin, 1985

9.0 REFERENCES

Crampin, S., 1985, Evaluation of anistoropy by shear-wave splitting, Geophysics, **50**, 142-152.

Dong, Z., and G. A. McMechan, 1993, 3D prestack migration in anisotropic media, Geophysics, **58**, 79-90.

Gelinsky, S., and S. Shapiro, Low Frequency Anistoropy of Layered Media, as presented at the 1995 EAEG, Glasgow, Scotland.

Gibson, R.L., and M., Toksoz, 1990, Permeability estimation from velocity anistoropy in fractured rock: J. Geophys. Res., **95**, 15 643-15 655.

Mallick, S., and L.N. Frazer, 1991, Reflection/transmission coefficients and azimuthal anistoropy in marine seismic studies, Geophys. J. Inter., **105**, 241-252.

O'Connell, J.K., Kohli, M., and S. Amos, 1993, Bullwinkle: A unique 3D experiment, Geophysics, **58**, p. 167-176.

Martin and Davis, 1987, Shear wave birefringence: a new tool for evaluating fractured reservoirs, The Leading Edge, vol. 6, no. 10, pp. 22-28).

APPENDIX: 3D SEISMIC MODELING

R 94 W

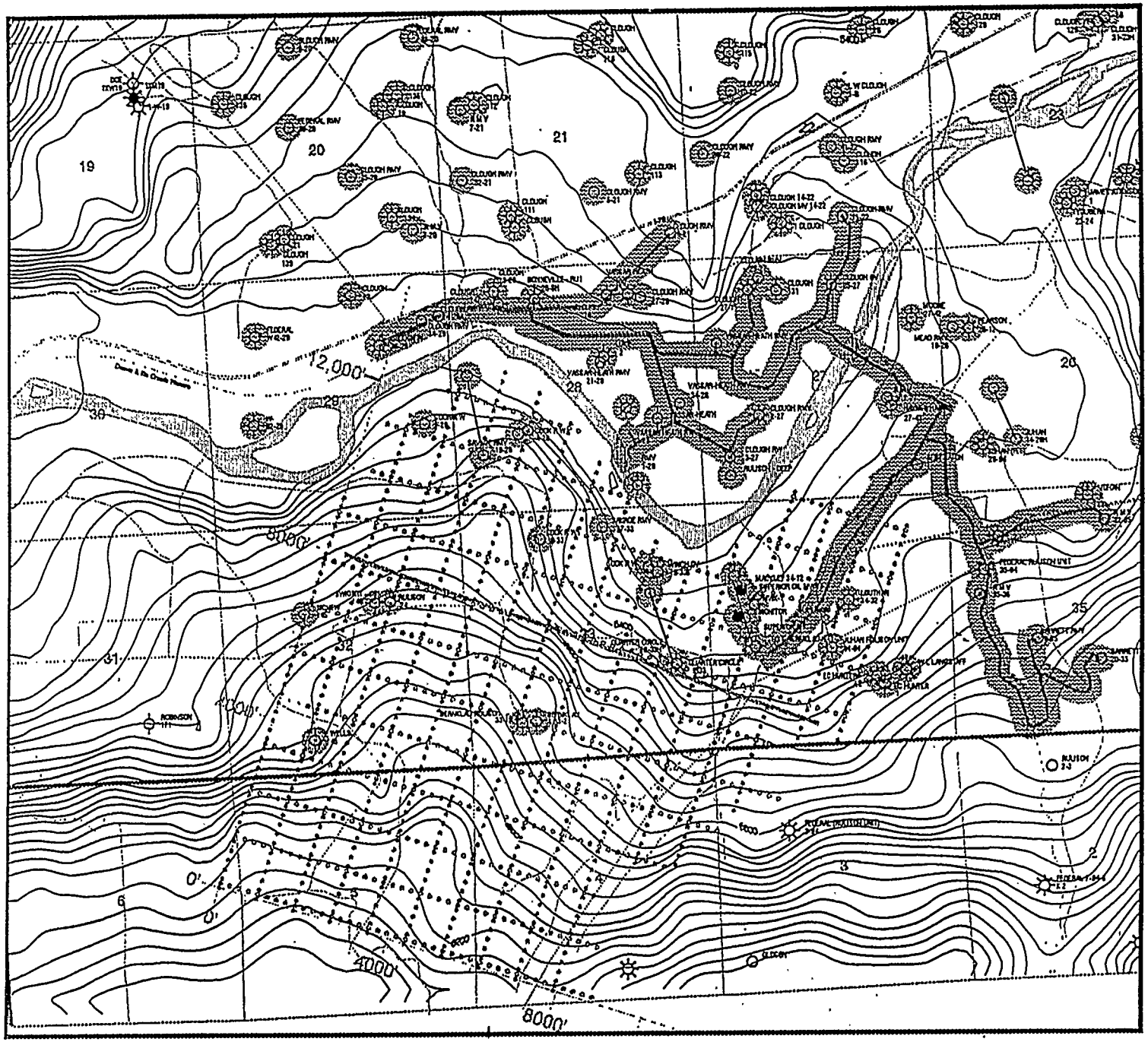

T 6 S

T 7 S

3D Receivers
3D Shotpoints
2D Shearwave
300' Radial Exclusion Zones
Pipeline
Power Transmission Lines

Topography of Rulison Field
Contour Interval: 40 feet

0.2 0. 0.2 0.4 0.6 0.8 1.
miles

Rulison Field
So. Piceance Basin, Colorado

0 - 10000Feet [45-135]

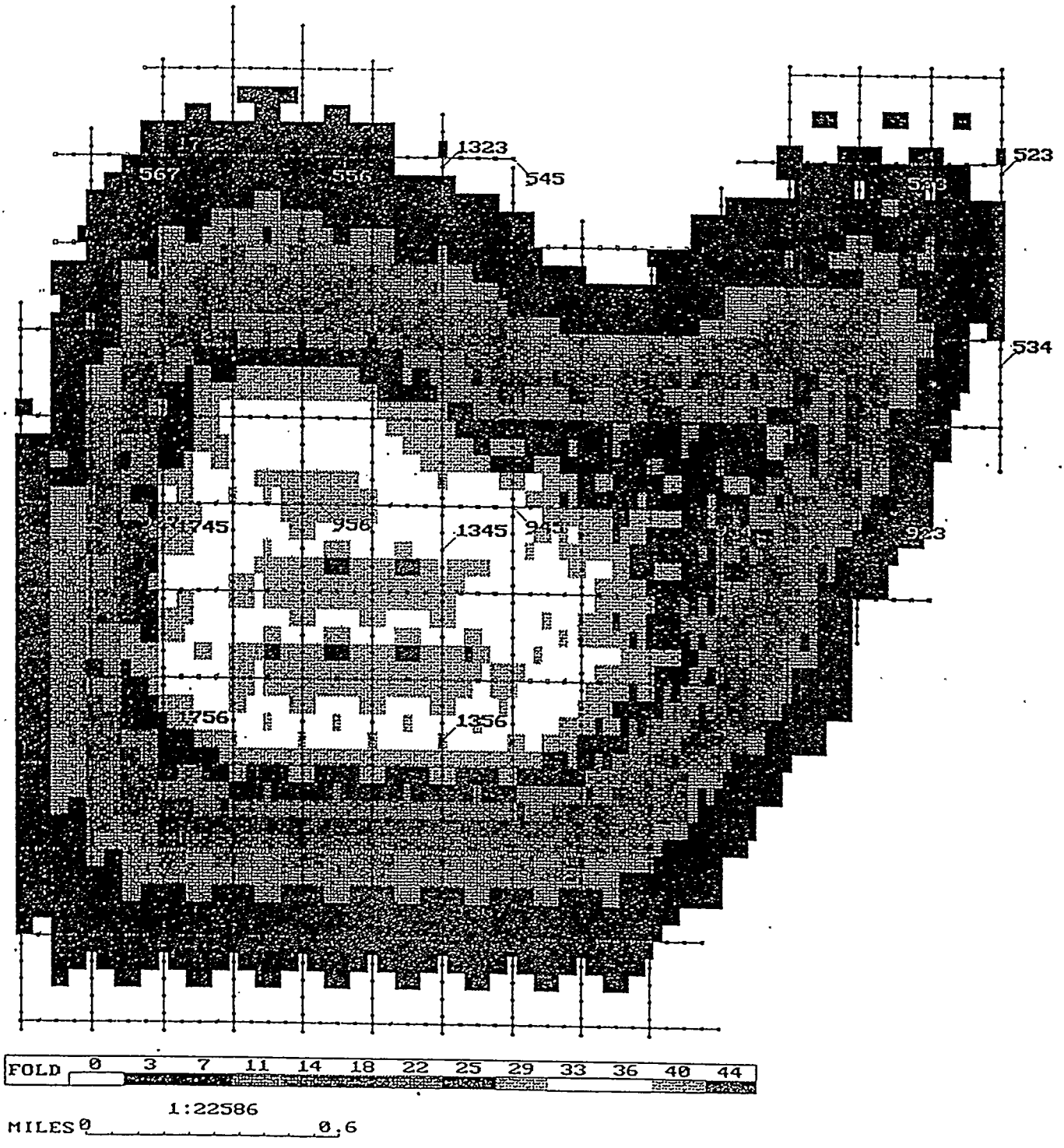

0 - 10000Feet [135-225]

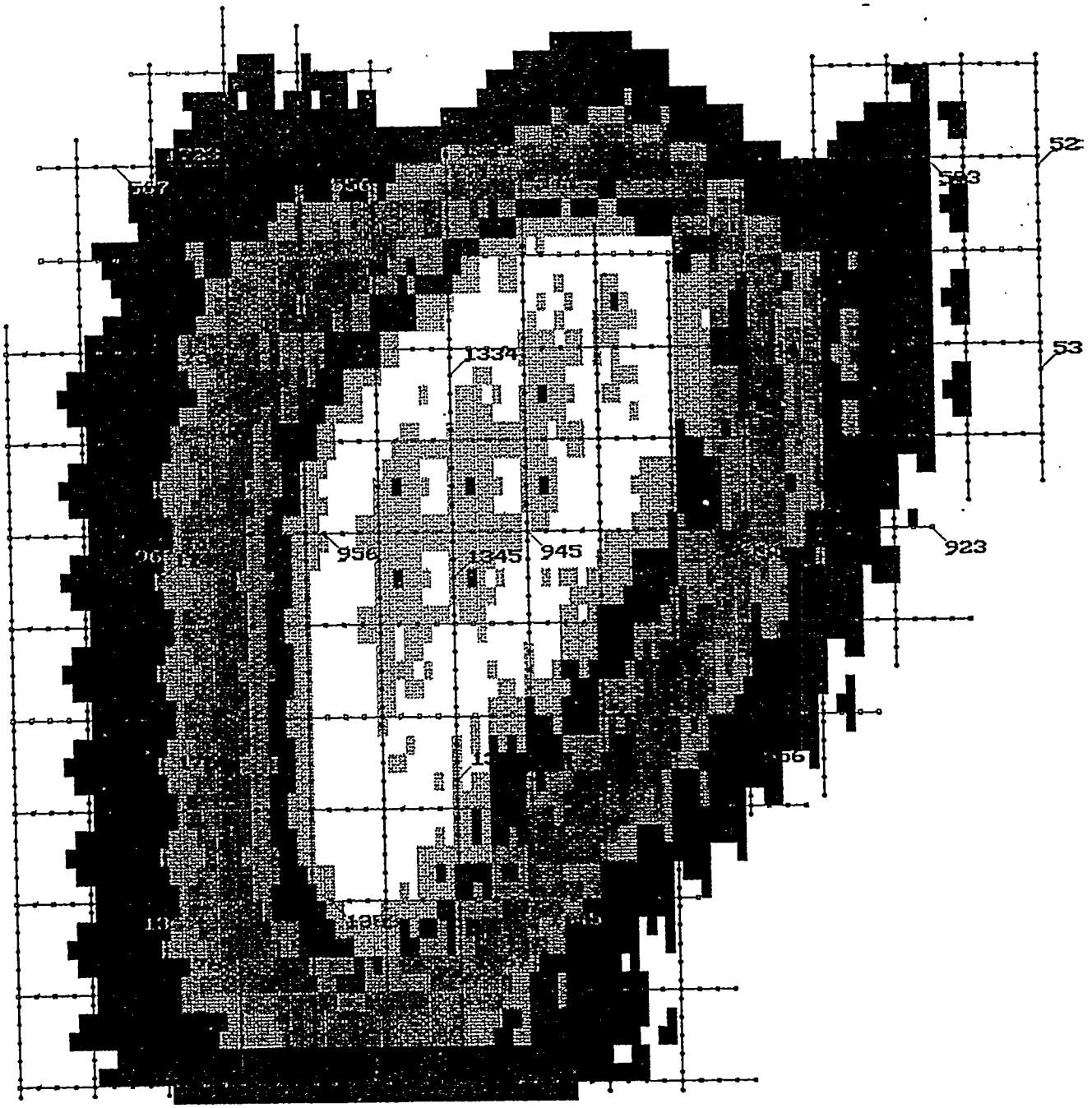

1:22586

MILES 0 0,6